Chapter 1

Time Dependent Mechanical Behavior of Hydrated Biological Tissues

1.1 Swelling and Deformational Behavior of Tissues: Experimental Observations

Characterization of the swelling of hydrated tissues is often a critical link in understanding the role of individual molecular constituents in the tissue's overall structure and mechanical behavior. Measurement of the *kinetics* of swelling can also help to delineate the mechanisms and rate-limiting processes that relate molecular level structure to macro-continuum biomechanics of tissues.

It is known that enthalpic and entropic effects, long-range electrostatic forces, as well as specific intra- and intermolecular crosslinkages, are among the interactions that can significantly affect the rheological behavior of biological tissues. For example, proteoglycans (PG) and their ionized glycosaminoglycan (GAG) constituents are primarily responsible for the osmotic swelling pressures of connective tissues at physiological pH. This swelling is crucial to the tissue's ability to withstand compressive mechanical loads in vivo. Urban et al[1] have pointed out that PG concentrations are higher in cartilagenous tissues than other connective tissues: PG account for $\sim$5% of the net wet weight in human femoral head cartilage and higher in the nucleus of the disc, compared to $\sim$0.1 – 1% in tendon and the loose connective tissue of umbilical cord (Wharton's jelly). Therefore, cartilagenous tissue would be expected to have a

[1]Urban, J.P.G., Maroudas, A., Bayliss, M.T., and Dillin, J., Biorheology, 16, 447, 1979.

higher osmotic swelling pressure. However, when excised specimens of articular cartilage, disc, and umbilical cord are placed in identical physiological saline, the cartilage swells by only 1-2%,[2] the disc may swell by 100% (annulus) to 250% (nucleus)[2] and native umbilical cord strips may well swell 50-100% beyond their in vivo wet weight. Thus, it is apparent that the content of fixed charge groups alone is only one of many factors that controls tissue swelling. The size and arrangement of collagen fibrils, chemical crosslinkages, mechanical entanglements, and other factors all play a role in determining the ultrastructure and equilibrium volume of a given tissue.

1.1.1 Measurement of Non-Equilibrium Tissue Volumetric Changes

While measurement of equilibrium hydration of tissues can lead to significant insight into tissue ultrastructure, *non-equilibrium* experiments and models are essential to the understanding of the *mechanism of tissue volumetric changes* and the chemical, mechanical and electromechanical rate processes that may govern transient tissue deformations. Such experiments have led to new information regarding the interaction between macromolecular constituents within a tissue. Non-equilibrium swelling behavior has been studied extensively in cornea,[3,4,5] tendon and reconstituted collagen fibers,[6,7], and many other tissues.

When the bath composition (e.g., ion concentrations, pH, etc.) of a specimen is altered, several nonequilibrium rate processes may occur simultaneously. The kinetics of each rate process can be approximated by a time constant associated with a linearized model. Important rate processes and their associated time constants include:

1. Diffusion of mobile ions within the matrix: $\tau_{\text{diff}} \sim \delta^2/D_i$; Chemical diffusion kinetics can be characterized by a time constant proportional to the square of the specimen thickness δ and inversely proportional to ion diffusivity D_i.[8].

2. Diffusion-limited binding of ions to matrix macromolecular sites:

[2]Maroudas, A., The Joints and Synovial Fluid, Vol. II, Sokoloff, L., Ed, Academic Press, New York, 1980, 240

[3]Elliott, G.F., Goodfellow, J.M., and Woolgar, A.E., J. Physiol., 298, 453, 1980.

[4]Hedbys, B.O., Mishima, S., and Maurice, D.M., Exp. Eye Res. 2, 99, 1963.

[5]Hodson, S., Wigham, C., Williams, L., Mayes, K.R., and Graham, M.V., Exp. Eye Res., 32, 353, 1981.

[6]Nussbaum, J.H., and Grodzinsky, A.J., J. Membrane Science, 8, 193, 1981.

[7]Lai, W.M., Hou, J.S., Mow, V.C., J Biomechanical Eng., 113, 245, 1991

[8]Crank,J.,The Mathematics of diffusion,2nd ed., Clarendon Press, Oxford,1975.

$\tau_{\rm dr} \equiv (\tau_{\rm diff})[1+R]$; Diffusion-limited chemical reactions can significantly impede the transport of mobile species into the matrix, as represented by the parameter R[9].

3. Readjustment of local (double layer) electric fields and forces: $\tau_{\rm ch.rel.} \sim \epsilon/\sigma$; Readjustment of local electric fields within the matrix, after an instantaneous change in the ionic content of the interstitial fluid, is proportional to the ratio of the interstitial fluid permittivity ϵ to its conductivity σ.[10] $\tau_{\rm ch.rel.}$ varies from $\sim 10^{-5} - 10^{-6}$ sec in bone,[11] with its relatively low fluid content, to 10^{-9} sec in tendon[24] and cartilage.[8] Charge relaxation times are so short that this process will never be rate-limiting for swelling of macroscopic tissues having dimensions δ much greater than a Debye length ($\sim$ 1nm)!

4. Mechanical readjustment (swelling) of the tissue matrix: $\tau_{\rm matrix} \sim \delta^2/(Hk)$; This process involves elastic reconfiguration of the matrix molecules simultaneously with relative fluid flow into or out of the matrix. The mechanical swelling of polymer gels[12] and connective tissues such as cartilage[13] and cornea[14] has been described in the small strain limit by a time constant proportional to the hydraulic permeability k and the elastic modulus H (tensile, compressive, etc.) of the matrix. When the intrinsic viscoelastic behavior of the solid matrix is important, yet another time constant would be appropriate.

5. Electrodiffusion: $\tau_{\rm ed} \equiv \tau_{\rm diff}[1+(E_o\delta/2\pi V_T)^2]^{-1}$; When an electric field E_o is applied across a tissue or a membrane of thickness δ, $\tau_{\rm ed}$ is the time needed for the establishment of a new equilibrium profile of mobile ion concentration within the tissue[15]. The new concentration profile represents a competition between ion migration through an applied voltage drop $E_o\delta$ and ion diffusion represented by the "thermal voltage" $V_T \equiv RT/F$ (assuming no binding reactions occur).

A comparison of the magnitudes of the above time constants can give valuable insight into the *mechanism* that controls swelling in different tissues. Based upon published experimental data and theoretical observations, The major conclusions are:

1. In relatively high modulus, soft connective tissues such as tendon and cartilage it has been discovered that $\tau_{\rm matrix} \ll \tau_{\rm diff}$. That is, electromechanical and

[9]Crank,J.,The Mathematics of diffusion,2nd ed., Clarendon Press, Oxford,1975.
[10]Stratton, J.A., Electromagnetic Theory, McGraw-Hill, New York, 1941
[11]Johnson, M.W., Chakkalakal, R.A., Harper, R.A., and Katz, J.L., J. Biomech., 13, 437, 1980.
[12]Tanaka, T. and Fillmore, D.J., J. Chem. Phys., 70, 1214, 1979.
[13]Mow, V.C., Kuei, S.C., Lai, W.M., and Armstrong, C.G., J. Biomech. Eng., 192, 73, 1980
[14]Friedman, M.H., J. Theor. Biol., 30, 93, 1971.
[15]Arndt, R.A. and Roper, L.D., Physical Biological Sciences Misc., Blacksburg, Va.

osmotic swelling (deswelling) induced by changes in bath neutral salt concentration occurs at least as rapidly as chemical diffusion. It was concluded that salt diffusion appeared to be the rate-limiting mechanism for swelling in such experiments.

2. In connective tissues with a lower modulus (e.g corneal stroma) and/or lower permeability, measurements have shown that $Hk \ll D_i$ ($\tau_{\text{diff}} \ll \tau_{\text{matrix}}$)[18,19,20,21]. The same would be expected for the nucleus of the disc, although this author has not yet seen such data. For tissues in which $\tau_{\text{diff}} \ll \tau_{\text{matrix}}$, changes in external bath concentration will chemically equilibrate with the interstitial fluid much faster than subsequent mechanical swelling (deswelling). In such cases, the observed swelling kinetics provides a direct measure of the product of the tissue's elastic modulus and hydraulic permeability, as long as solid phase matrix viscoelasticity is not important.

3. Conversely, for tissues in which $\tau_{\text{matrix}} \ll \tau_{\text{diff}}$, free swelling kinetics are dominated by chemical processes (i.e. the slowest, rate-limiting process). In such cases, the measured swelling kinetics may be invaluable as a quantitative, nondestructive measure of certain biochemical properties, such as diffusion-limited binding (τ_{dr}) of Ca^{++} and other ions to connective tissues.

4. The kinetics of swelling brought about by electrodiffusion-induced changes in intra-tissue salt concentration should be governed by τ_{ed} as long as $\tau_{\text{matrix}} \ll \tau_{\text{ed}}$. This was recently demonstrated with collagen membranes: a sinusoidal transmembrane field produced sinusoidal changes in isometric stress whose frequency response correlated with electrodiffusion-controlled variations in intramembrane NaCl concentration.

A final caution concerning swelling experiments is necessary. Prolonged swelling of connective tissues may lead to proteoglycan loss and other degeneration processes, even when enzymatic inhibitors are used. A micrograph of corneal stroma with edema (Chapter 1.4) shows an even more drastic matrix degradation. For tissues such as disc, cornea and umbilical cord which may undergo large changes in hydration, the measured swelling kinetics may be dominated by artifactual tissue breakdown. In such cases, the H and k predicted from such data would have little meaning.

1.2 Linear Poroelastic Behavior of Tissues: Theories and Experiments

We have seen that the nonequilibirum rheological behavior of biological tissues is the result of complex interactions involving both the interstitial fluid and the extracel-

lular solid matrix constituents. In some cases, single phase viscoelastic models (e.g., lumped parameter spring/dashpot models) may be able to characterize tissue mechanics within limited ranges of stress, strain, and time (frequency). For example, cyclic testing of tendons and ligaments in tension has been described by the quasi-linear viscoelastic theory of Fung [Woo et al., 1981, Y.C. Fung, 1982]. Tensile testing of connective tissues is sometimes dominated by the solid collagen fiber constituents and, therefore, flow of water may be somewhat less important. Similarly, the dynamic shear behavior of soft tissues may involve little or now flow of interstitial water relative to the solid matrix, especially at very small strains. Hence, any "viscoelastic" behavior that may be observed may be ascribed to the solid phase of the tissue.

However, the compressional behavior of hydrated soft tissues must necessarily involve flow of fluid through the extracellular matrix. The resulting frictional interactions between fluid and solid phases lead to the remarkably different rheological properties of such tissues. We will see that the time dependent "poroelastic" displacement profile is no longer uniform when relative fluid flow is important, as was assumed for the case of purely solid phase viscoelasticity (see Chapter 1.2). Thus, in addition to a temporal phase delay between stress and strain at any point within the tissue, there is also a spatial phase delay between the displacement from one point in the tissue to the next. That is, the displacement profile within the tissue is found, in general, to be described by the solution to a partial differential equation in space and time.

Various poroelastic and mixture theories have been successfully applied to describe the deformational behavior of soft connective tissues, gels, geophysical materials, soils, and other materials composed of a multiple of fluid and solid phases. The following discussion will focus on the fundamental laws that can be combined to formulate a general model for the mechanical and electromechanical behavior of soft tissues. In addition, the influence of the chemical environment on the stress-strain and material properties of such tissues will be included. For simplicity, we focus on isotropic, homogeneous, linear material behavior and, to exemplify a class of approaches, utilize a simple poroelastic approach similar to that of Biot and coworkers.

1.2.1 Equillibrium Total Stress Constitutive Relation

In many tissues, there are distinct molecular constituents that are separately responsible for different components of the total swelling stress. For example, in articular cartilage at physiological pH, it is accepted that the repulsive interactions between the charge groups of the proteoglycan aggregates provide the positive swelling force, while the elastic recoil of the stretched collagen fibrous network maintains tissue integrity (Maroudas, 1979). In what follows, we develop a constitutive relation for the total

swelling stress. Experiments will also be described that characterize the contribution of electrical forces to the material properties that make up this constitutive relation.

In general, the total swelling stress is made up of several components that result from distinct physical interactions (Flory, 1953), including:

1. a component due to stretching of the marcomolecular chains comprising the interconnected solid matrix. This component opposes swelling and its magnitude increases as swelling increases.

2. a component due to electrostatic (Donnan osmotic) interactions. This component can be interpreted at the molecular level as the result of double layer repulsive forces between charged constituents of the tissue. Alternatively, at the macro-continuum level, this component can be interpreted as an osmotic pressure resulting from the increased concentration of counterions that must be present in the tissue to preserve electroneutrality. These are one and the same phenomena. The magnitude of this component of the swelling stress decreases with increased swelling, increased external ion concentrations, or decreased fixed charge density.

3. a component due to interactions between the matrix macromolecules and the solvent. This component accounts for the affinity between the matrix and the solvent. For "good" solvents, the matrix tends to imbibe fluid and increase swelling. Similarly, the matrix tends to resist swelling in "poor" solvents.

4. a component due to the thermal motion of the matrix macromolecular segments, often referred to as polymer excluded volume effects. This component tends to swell the network, and its magnitude decreases as swelling increases.

In developing a constitutive law for total stress, we will include on tissue swelling behavior that is mediated by electrical interactions between the charged constituents of the solid tissue matrix. Changing ion concentrations in the tissue bathing solution alters the electrical repulsive forces between these constitutents by changing the electrical interaction distance (Debye length) within the tissue. In an experiment in which the deformation is held constant, the altered electrical repulsive forces give rise to a change in swelling stress and a concomitant change in the measured stress required to keep the deformation constant. Conversely, when the stress on the tissue is held constant, a change in salt concentration results in a change in tissue deformation as the charged constituents alter their relative spacing in response to the modified repulsive forces.

The total stress T_{ij} for a homogeneous, isotropic linear tissue sample in equilibrium can be expressed by a modified form of the generalized Hooke's law in terms

of the strain ϵ_{ij}, concentration dependent Lame constants $G(c)$ and $\lambda(c)$ and the chemical stress $\beta(c)$ as

$$T_{ij} = 2G(c)\epsilon_{ij} + \{\lambda(c)\epsilon_{kk} - \beta(c)\}\,\delta_{ij} \tag{1}$$

where the chemical stress $\beta(c)$ represents the chemical analog of the thermal stress in the thermoelasticity. It is postulated in Eq. (1) that three concentration dependent material properties are required to completely describe the chemical modulation of swelling behavior for such a homogeneous, isotropic tissue. (To account for tissue anisotropy, Eq. (1) must be generalized and β may vary with direction).

For the uniaxial confined compression geometry of Figure 8.2.1, Eq. (1) can be written in terms of two concentration dependent material parameters as

$$\sigma = -T_{zz} = -[2G(c) + \lambda(c)]\epsilon_{zz} + \beta(c) = H(c)\epsilon + \beta(c) \tag{2}$$

where $H = 2G + \lambda$ is the bulk longitudinal modulus (confined compression modulus), and the uniaxial stress σ and strain $\epsilon(= -\epsilon_{zz})$ are defined positive in compression. For a homogeneous sample in equilibrium at concentration c, a mechanical stress equal to the swelling stress $p(c, \epsilon) \equiv H(c)\epsilon + \beta(c)$ is required to keep the tissue at a given thickness in the configuration of Figure 8.2.1.

The bulk longitudinal modulus H can be measured at any concentration c_o by applying an increment in compressive stress, $\Delta\sigma$ (strain $\Delta\epsilon$), as shown in Figure 8.2.2. H varies with salt concentration because the resistance of the tissue to deformation depends on the extent of electrical interaction between the charged macromolecules that comprise the solid tissue matrix.

The origin of the concentration dependent chemical stress β can be best understood in the following way. A tissue sample in equilibrium with a bath whose salt concentration is large enough to shield electrical interactions is used to define the reference thickness for the sample, as shown in Figure 8.2.3a. When the bath concentration is decreased, electrical repulsive forces between the charged constituents of the solid matrix are increased. When the tissue sample is allowed to swell in the thickness direction, the thickness of the sample increases (Figure 8.2.3b), thereby stretching the constraining chains of the matrix. Equilibrium is reached when the increased electrical repulsive forces are balanced by the constraining force of the stretched network. The stress σ required to compress the sample back to its strain free state (Figure 8.2.3c) as defined by the reference thickness λ_{ref}, defines the chemical stress $\beta(c)$. β is the stress that would be measured in equilibrium if the sample was held at its reference thickness while the salt concentration was decreased.

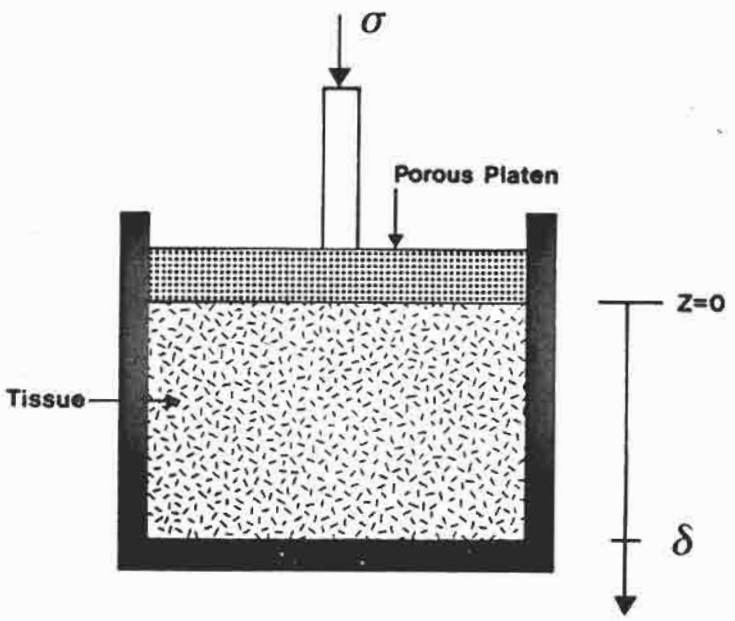

Figure 1.2.1: Uniaxial Confined Compression

An example of show data for the NaCl concentration dependence of H and β, measured for bovine corneal stroma and articular cartilage is shown in Figure 8.2.4a,b (Eisenberg and Grodzinsky, 1985). The modulus of bovine cartilage disks in uniaxial confined compression was found to be 1.1 MPa at 0.005 M NaCl, 0.55 MPa at 0.15 M NaCl, and 0.27 MPa at 1.0 M NaCl. The observed decrease in the modulus with increased concentration can be attributed to the electrostatic shielding of the proteoglycan charge groups by counterions. The relative insensitivity of H to changes in NaCl concentration at the highest concentrations tested suggests that electrostatic and Donnan osmotic forces are almost completely shielded in these specimens in 1.0 M NaCl. By comparing the modulus at 0.15 M NaCl to the modulus at 1.0 M NaCl it can be concluded that electrostatic repulsive interactions account for at least half of the modulus at physiological ionic strength in bovine articular cartilage.

The chemical stress for bovine articular cartilage shows a more rapid decrease with concentration. Here again, the electrostatic shielding effect of increased NaCl concentration results in less stress being required to keep the tissue at its reference volume. The chemical stress is even more important to the swelling behavior of bovine corneal stroma for the strain levels applied in this study, as can be seen by comparing the modulus and chemical stress components of corneal swelling stress. This is consistent with the fact that corneal stroma is known to swell for more extensively than articular cartilage (Hedbys and Dohlman, 1963, and Maroudas, 1980).

Based on Donnan osmotic theory alone, one would expect that changes in the electrostatic contribution to H and β would begin to decrease significantly as the concentration of the bath exceeded the average fixed charge density of the tissue. (The charge density of bovine femoropatellar groove cartilage specimens is about - 0.2 M while that of bovine corneal stroma is - 0.05 M). While the data of Figure 8.2.4 qualitatively supports this notion, it is apparent that the concentration dependence is more complex. The difference in the concentration dependence of H and β for a given tissue may be the consequence of tissue ultrastructure.

Similarly, the marked difference in the material properties H and β of cartilage and corneal stroma cannot be interpreted solely on the basis of fixed charge density. While corneal stroma has about three times fixed charge than articular cartilage, corneal stroma specimens swell far more than cartilage under no load conditions. This due primarily to the differences in the morphology and ultrastructure of the extracellular matrix of these tissues. In normal articular cartilage, the tendency of the proteoglycans to hydrate is well constrained by the collagen network. In corneal stroma, the proteoglycans help to organize collagen fibrils in a precise parallel array within each 2 μm thick lamella, but staggered in orientation from one lamella to the next within the $\sim 800\mu$m stroma. The resulting highly organized collagen structure helps to optimize corneal transparency and prevents radial swelling (in the plane of the cornea), but allows such significant swelling in the thickness direction that

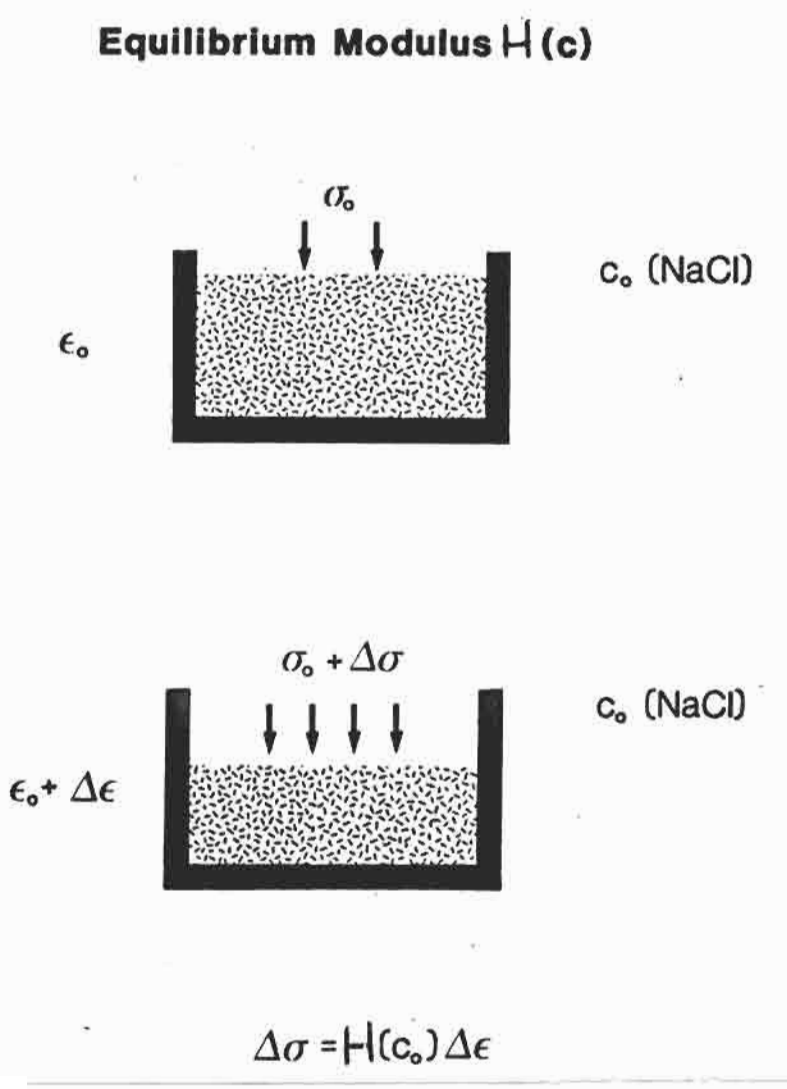
Equilibrium Modulus H (c)
σ_o
c_o (NaCl)
ϵ_o
$\sigma_o + \Delta\sigma$
c_o (NaCl)
$\epsilon_o + \Delta\epsilon$
$\Delta\sigma = H(c_o)\,\Delta\epsilon$

Figure 1.2.2:

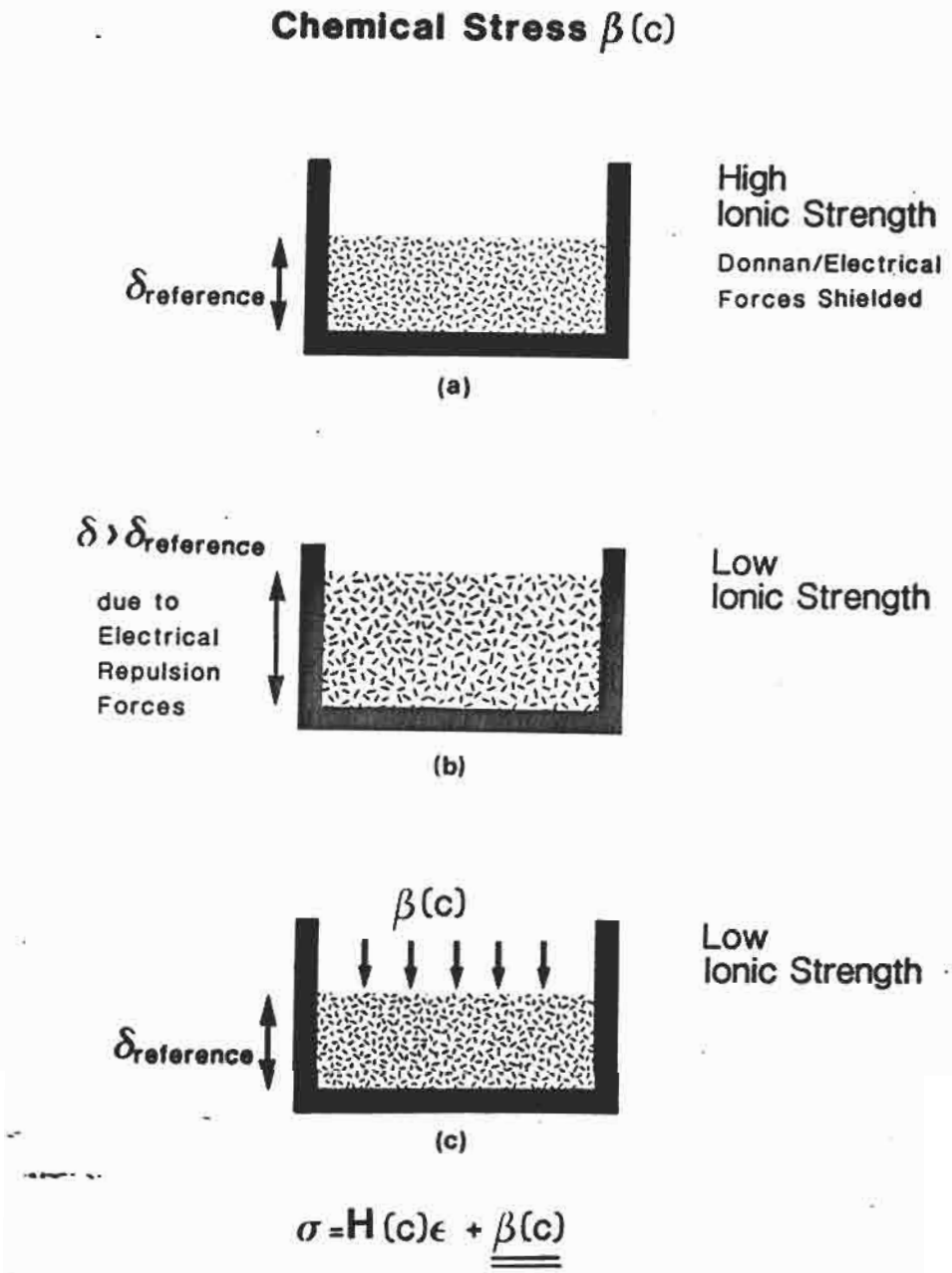
Chemical Stress $\beta(c)$
$\delta_{reference}$
High
Ionic Strength
Donnan/Electrical
Forces Shielded
(a)
$\delta > \delta_{reference}$
due to
Electrical
Repulsion
Forces
Low
Ionic Strength
(b)
$\beta(c)$
$\delta_{reference}$
Low
Ionic Strength
(c)
$\sigma = H(c)\epsilon + \underline{\underline{\beta(c)}}$

Figure 8.2.3

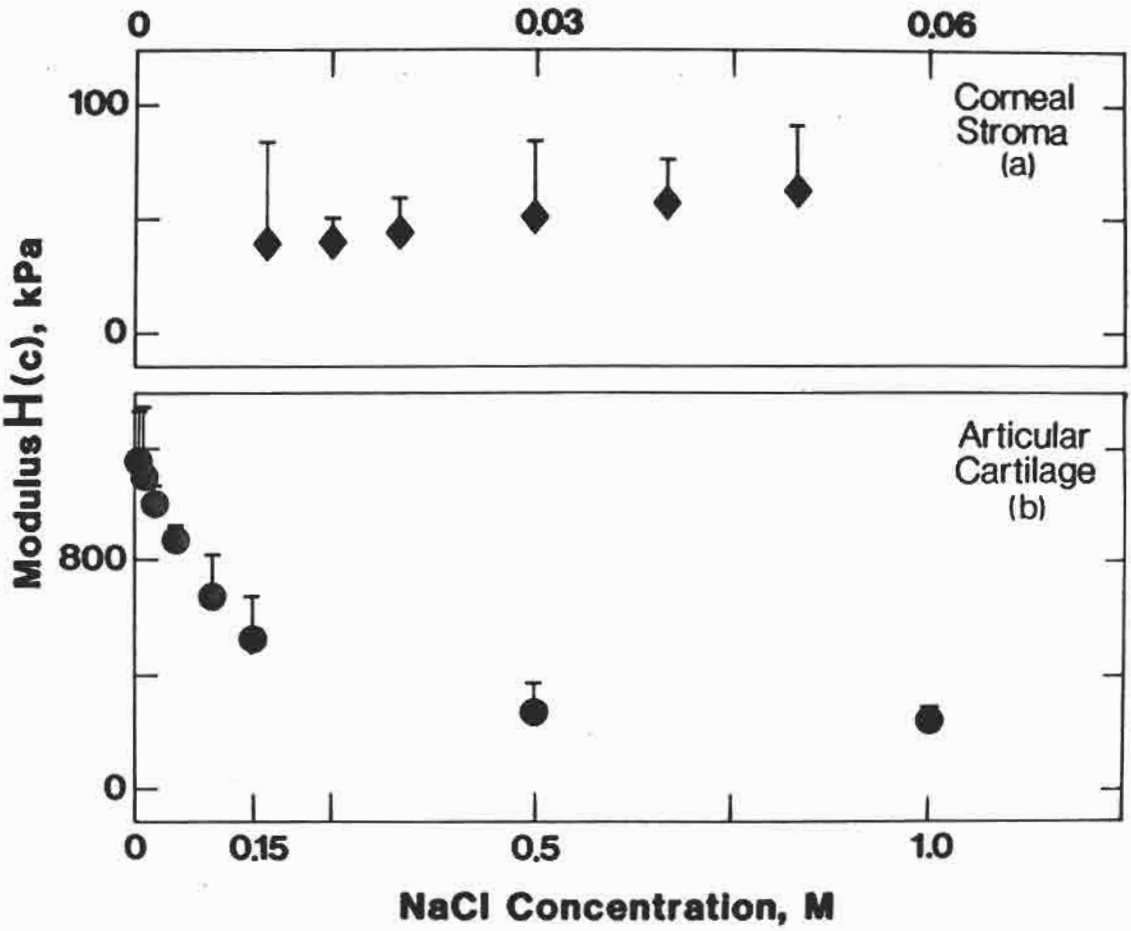
0
0.03
0.06
100
0
Corneal
Stroma
(a)
Articular
Cartilage
(b)
800
0
0
0.15
0.5
1.0
Modulus H(c), kPa
NaCl Concentration, M

Figure 1.2.4: (a)

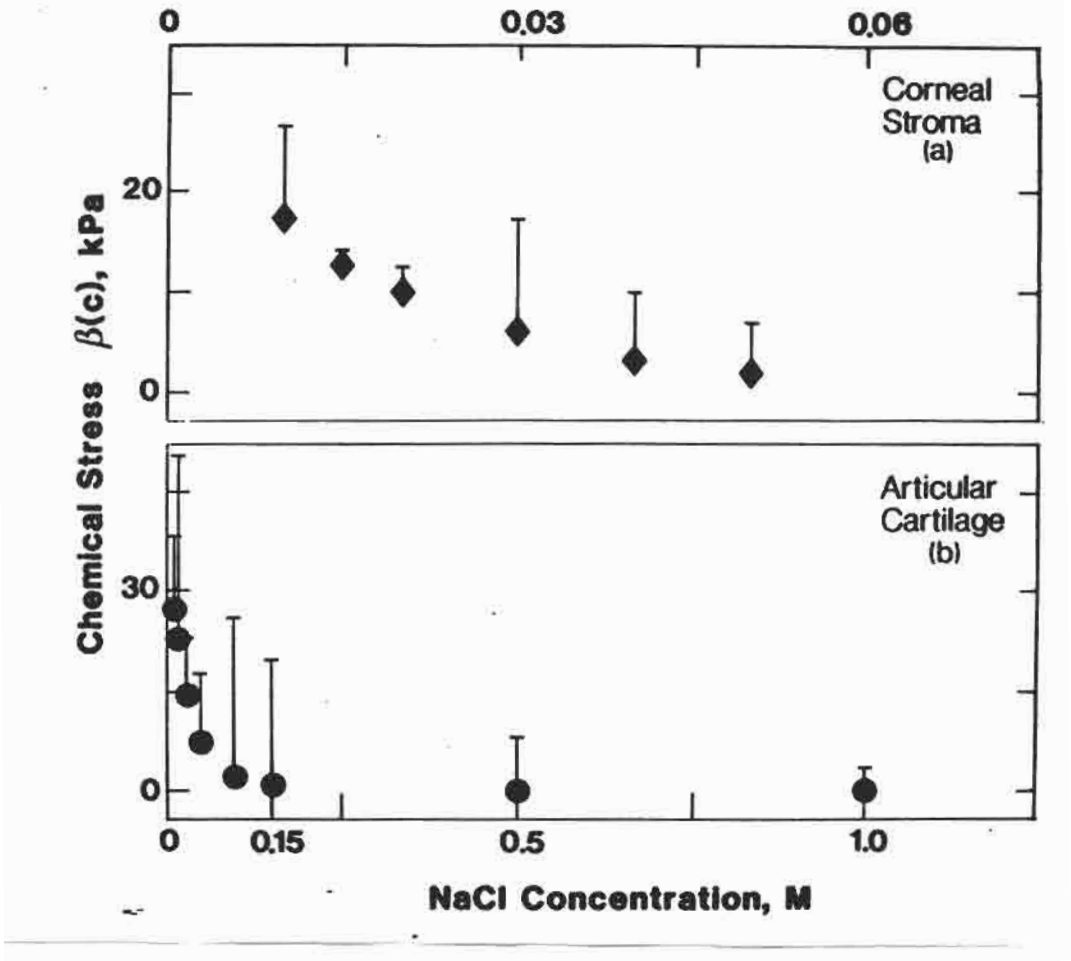
0
0.03
0.06
Corneal
Stroma
(a)
20
0
Articular
Cartilage
(b)
30
0
0
0.15
0.5
1.0
Chemical Stress β(c), kPa
NaCl Concentration, M

Figure 1.2.4: (b)

an active endothelial cell pump is required in viiivo to express water and thereby maintain normal corneal hydration (Mishima and Kuda, 1967).

1.2.2 Darcy's Law for Fluid Flow in Porous Media

We assume that the fluid is incompressible and intrinsically inviscid; frictional (viscous) interactions between the fluid and solid matrix in the tissue are described by Darcy's Law, which relates the fluid flux to the gradient in total fluid pressure at any point within the material. Because the tissue is charged, osmotic (π) as well as hydrostatic (P) pressure gradients must be included in Darcy's law. In equilibrium, when there is no flow anywhere inside the tissue or across the tissue/bath interface, $(P-\pi)_{\text{tissue}} = (P_o - \pi_o)$, where P_o and π_o are the hydrostatic and osmotic pressures in the external bath. The hydrostatic pressure P_o can be set equal to zero without loss of generality (free draining). However, the osmotic pressure π_o cannot be set to zero for finite bath concentrations. Because of this asymmetry between the hydrostatic pressure P and the osmotic pressure π, it is convenient to define the osmotic pressure difference.

$$\Delta\pi(z,t) \equiv \pi(z,t) - \pi_o \tag{3}$$

Within the tissue, fluid flow is related to the gradient in the pressure difference $(P - \Delta\pi)$ (Katchalsky and Curran, 1965). With the fluid pressure defined as $P_f = (P - \Delta\pi)$, the fluid velocity $\boldsymbol{U}$ is related to the gradient in P_f by Darcy's law:

$$\boldsymbol{U} = -k\nabla P_f \tag{4}$$

where $\bar{U}$ is the total area averaged relative flow of fluid with respect to the solid and k is the tissue hydraulic permability. Implicit to the fluid flow law of Eq. (4) is that inertial effects are negligible, a reasonable assumption for the known fluid mass density, time rates of change (frequencies), and frictional damping forces that are of interest. For the case where inertia is important, Darcy's law would be replaced by a more general statement of conservation of momentum for the fluid (for example, see Friedman, 1970, 1971).

1.2.3 Nonequilibrium Stress-Strain Constitutive Law

Under nonequilibrium conditions, a fluid pressure term must be added to Eq. (1) to account for the effect of fluid flow on the total T_{ij}. The total stress T_{ij} can then be expressed as

$$T_{ij} = 2G(c)\epsilon_{ij} + \{\lambda(c)\epsilon_{kk} - \beta(c) - P_f\}\,\delta_{ij} \tag{5}$$

This expression is analogous to the general relations given by Rice and Cleary and Biot for porous media in the limit of incompressible fluid and solid constituents, although the chemical stress β and the chemical dependence of the material constants G and λ were not included in those developments. The total stress T_{ij} is also equivalent to the sum of T^s_{ij} of the solid and T^f_{ij} of the fluid in the mixture model by Mow et al (1980).

For the uniaxial confined compression geometry of Figure 8.2.1, Eq. (2) becomes

$$\sigma = H_A(c)\epsilon + \beta(c) + P_f \tag{6}$$

1.2.4 Conservation of Mass

Conservation of mass for the case of incompressible solid and fluid consitutents takes the form

$$\nabla \cdot \boldsymbol{v}_f + \alpha \nabla \cdot \boldsymbol{v}_s = 0 \tag{7}$$

where α is the solid volume to liquid volume ration (V_s/V_f) and $\boldsymbol{v}_f$ and $\boldsymbol{v}_s$ are the local (lab frame) velocities of the fluid and solid constituents defined in terms of the relative velocity $\boldsymbol{U}$ and the porosity ϕ as:

$$\boldsymbol{U} = (\boldsymbol{v}_f - \boldsymbol{v}_s)\phi \tag{8}$$

In Eqs. (7) and (8), α and ϕ are related by $\phi = 1/(1+\alpha)$, since porosity is just $V_f/(V_f + V_s)$.

In the confined uniaxial geometry of Figure 8.2.1, Eq. (7) becomes

$$\frac{\partial U}{\partial z} = \frac{\partial \epsilon}{\partial t} \tag{9}$$

Since the strain $\epsilon = -\partial u/\partial z$, with solid displacement u related to v_s by $v_s = \partial u/\partial t$, Eq. (9) reduces further for the case when fluid is forced to move in only one direction opposite to the motion of the solid. For example, with an impermeable bottom surface at $z = \delta$ in Figure 8.2.1, compression of the tissue forces fluid to move upward such that equation Eq. (9) takes the form $U = -\partial u/\partial t$

In the absence of inertial effects, conservation of momentum requires that

$$\partial T_{ij}/\partial x_j = 0 \tag{10}$$

This is an excellent approximation for frequencies and strain rates of physiological interest. In uniaxial geometry, Eq. (10) becomes

$$\frac{\partial \sigma}{\partial z} = 0 \tag{11}$$

Eqs. (4) and (11) describe the relation between the total stress, fluid flow, displacement and swelling stress when the material properties are known. When the material properties depend on the ionic concentrations, the kinetics of the transition in the material properties induced by a change in the concentration of the external bath must also be examined in order to describe the evolution of the mechanical response. This will be described in a later section.

1.2.5 Summary

For the case of chemically homogeneous systems (no chemical transport or gradients in chemical species), Eqs. (4), (6), (9), and (11) constitute a complete description of tissue mechanics in terms of the unknowns σ, ϵ, U, and P_f in the uniaxial geometry of Figure 8.2.1. By extension, Eqs. (4), (5), (7), and (10) describe prorelastic deformations and flows in three dimensions. When the material properties (e.g., H, k, and β) depend on chemical environment, constitutive laws for the concentration dependence must be derived or measured (e.g., Figure 8.2.4).

In the next sections, we use the simple poroelastic model outlined above in a series of examples to describe the nonuniform deformation response and the dynamic

mechanical stiffness of hydrated biological tissues. We then extend the model to incorporate electrokinetic transduction interactions such as deformation induced streaming potentials and electrical current-induced mechanical stress. Finally, we compare some experimental results and theoretical predictions for the manner in which changes in ionic environment lead to altered tissue stiffness in compression and tension.

1.3 Hydraulic Permeability, Dynamic Stiffness, and Electrokinetic Behavior of Tissues Modeled as Hydrated Poroelastic Media

1.3.1 Macrocontinuum Approaches

Fluid flow and electrokinetic transduction in biological tissues and natural and synthetic membranes have been modeled by non-equilibrium thermodynamic relations cast in the lumped parameter form of Eq. (1) or in the continuum form of Eq. (2). Eq. (1) relates one dimensional fluid and current flows to *transmembrane* pressure and potential drops (see Chapter 1.4), while Eq. (2) applies to the total area-averaged, one dimensional flows and pressure and potential gradients *within* the tissue:

$$\begin{bmatrix} \vec{n} \cdot (\vec{v} - \vec{v}_m) \\ \\ \vec{n} \cdot \vec{J}' \end{bmatrix} = \begin{bmatrix} L_{11} & L_{12} \\ \\ L_{21} & L_{22} \end{bmatrix} \begin{bmatrix} \Delta P \\ \\ \Delta V \end{bmatrix} \tag{1}$$

$$\begin{aligned} U_z(z) &= -k_{11}\frac{\partial P}{\partial z} + k_{12}\frac{\partial V}{\partial z} \\ J_z(z) &= +k_{21}\frac{\partial P}{\partial z} - k_{22}\frac{\partial V}{\partial z} \end{aligned} \tag{2}$$

Eqs. (1) and (2) apply to systems having negligible chemical concentration gradients. The k_{ij} of (2) are intrinsic material properties that depend on the electrical, mechanical and chemical properties of the tissue matrix. The matrix is assumed to be isotropic, but the k_{ij} may vary with z for the case of nonuniform material. For homogeneous, isotropic materials the phenomenological coefficients k_{ij} and L_{ij} are related by the specimen thickness δ: $\delta L_{ij} = k_{ij}$. The electrokinetic coupling coefficients may be modeled in terms of a macrocontinuum fixed charge density, $k_{12} =$

$k_{21} = \rho_m k$ (see Problem **??**), where $k = (k_{11} - [k_{12}k_{21}/k_{22}])$ is the open-circuit Darcy permeability, or in terms of a microcontinuum surface charge or ζ (zeta)-potential associated with individual matrix macromolecules.

Eqs. (1) and (2) constitute a phenomenological description of electrokinetic transduction, including streaming potentials ($-k_{21}/k_{22}$) first and second electroosmotic flow (k_{12}/k_{22} and k_{12}, respectively), and streaming current (k_{21}/k_{11}), as summarized by Katchalsky and Curran, (1965).

Maroudas (1969) was the first to measure steady-state streaming potential in articular cartilage, generated by a steady pressure difference applied across 400μm slices of tissue. She used a macroscopic, homogeneous fixed charge theory related to Eq. (1) to calculate the average charge density within the slab from the data. Experimental problems in such a steady-state measurement included concentration potentials due to stagnant films, and electrode offset drift. Subsequently, Maroudas suggested that a cation tracer method was simpler and more accurate.

It is not always appreciated that Eqs. (1) and (2) may be applied to time varying "quasistatic" forces and flows, as well as to the steady state. Several investigators have measured non-steady deformation-induced streaming potentials in connective tissues and blood vessel walls. A model of the form (2) can be fit to the data of experiments in sinusoidal steady state compression over a wide frequency range, as will be discussed below.

The electrokinetic equations (1) and (2) also demonstrate the very important influence of tissue fixed charge groups on hydraulic permeability. When there is no potential gradient ($\partial V/\partial z = 0$) the permeability is just k_{11} from Eq. (2a), and is called the "short circuit permeability". When fluid flow induces streaming potentials so that ($\partial V/\partial z$) is not zero, then the permeability under open circuit conditions is $k \equiv [k_{11} - (k_{12}k_{21}/k_{22})]$, which can be derived from Eq. (2a,b) with $J = 0$. The backflow term ($k_{12}k_{21}/k_{22}$) represents the electrical force exerted by the streaming potential ($\partial V/\partial z$) on the space entrained by the fluid phase, intending to reduce the flow and hence lower the effective permeability. The streaming potential field can be suppressed by increasing the salt concentration of the interstitial fluid. This fact provides an experimental method for testing the significance of the backflow term.

1.3.2 Creep and Stress Relaxation Revisited

(A comparison of single phase lumped element viscoelastic models with the predictions of poroelastic models)

1.3.3 Deformation Induced Streaming Potentials In Hydrated Tissues

The Streaming Potential-Versus-Piezoelectricity Controversy

Yasuda[16] first discovered that electrical potentials are generated when bone is bent. This property of bone was termed a piezoelectric effect.[17] Several extensive reviews[18,19,] have summarized the research on this fundamental electromechanical property and its possible function in growth and remodeling of tissues.

The piezoelectric mechanism received wide attention. Theories were derived for piezoelectricity in dry bone, in which the piezoelectric response was ascribed to the collagen phase since the crystal structure of the mineral hydroxyapetite is not of the class of piezoelectrically active materials.[20] Experiments characterized the dependence of deformation induced potentials in dry bone on frequency (1-1000 Hz), and the dependence on relative humidity in moist bone.

Investigators began to question whether the piezoelectric mechanism described the observed electromechanical behavior of *wet* bone under *physiological conditions.* The relatively fast dielectric charge relaxation times, estimated to be less than 50μsec, were not compatible with observations of slow decay rates for potentials observed in wet bone.[73] (Deformation-induced polarization charge would be screened by the ions of the interstitial fluid to within a few Debye lengths ($\sim$ 1nm) within a few charge relaxation time constants). It was then suggested that a streaming potential mechanism might be compatible with experimental data in wet bone. The effect of the interstitial fluid's concentration of NaCl, $CaCl_2$, and HCl on the magnitude and sign of steady-flow-induced potentials, and on potentials induced in bending beam and sinusoidal four-point bending geometries led research groups to suggest that a streaming potential mechanism is dominant. Changes in fluid viscosity also affected the potential in a manner consistent with a streaming mechanism.

Figure 8.3.1 depicts the streaming potential mechanism in terms of a macrocontinuum (a) and a microcontinuum (b) picture. The material contains fixed negative charge groups and an interstitial fluid containing an excess of positive counterions so that electroneutrality is preserved. When a solid Ag/AgCl reference electrode com-

[16]Yasuda, I., J. Kyoto Pref. Univ. Med., 53, 352, 1953.

[17]Fukada, E., Adv. Biophys., 6, 121, 1974.

[18]Bassett, C.A.L., The Biochemistry and Physiology of Bone,Vol. III, Bourne, G.H., Ed., Academic Press, New York, 1, 1971.

[19]Eriksson, C., The Biochemistry and Physiology of Bone, Vol. 4, Bourne, G.H., Ed., Academic Press, New York, 329, 1976.

[20]Brighton, C.T., Black, J., Friedenberg, Z.B., Esterhai, J.L., Day, L.J., Connolly, J.F., J. Bone Jt. Surg., 63-A,2. 1981.

presses the material against a porous Ag/AgCl electrode, fluid is forced through the porous electrode. Fluid entrainment of mobile ions produces a slight excess of counterions in the region of the porous electrode and a slight excess of unneutralized fixed charge groups at the other electrode. This charge separation produces the streaming potential. The microcontinuum model of Figure 8.3.1b pictures the balance of viscous and electrical shear stresses in the electrical double layer at the surface of a negatively charged solid particle. Here, fluid convection of counterions along the surface produces a streaming potential proportional to the double layer surface charge, or equivalently, the electrokinetic ζ-potential.

EXAMPLE: Deformation, Fluid Flow, and Electrokinetic Response of soft Tissue in Uniaxial Confined Compression

Deformation-induced potentials in soft tissues such as tendon, cartilage, and vessel walls have been measured. A macrocontinuum poroelastic theory for streaming potentials in soft tissues is summarized below. This model accounts for the dependence of the potential on the nonuniform fluid velocity profile within the tissue caused by dynamic or transient mechanical deformation of the tissue.

The theory incorporates the linear, nonequilibrium thermodynamic constitutive laws, Eq. (2), which relate the average fluid velocity $U_z(z)$ and current density $J_z(z)$ to the local pressure and potential gradients *within* the tissue. Figure 8.3.1a shows the coordinate frame of reference.

The current density J in Eq. (2b) is negligible when a high input impedance is used to measure the potential. Thus, $\partial P/\partial z$ can be written in terms of $\partial V/\partial z$ and Eq. (2a) becomes:

$$U_z = -k\left(\frac{k_{22}}{k_{21}}\right)\frac{\partial v}{\partial z} \tag{3}$$

To find the streaming potential measured between the positive electrode at $z = 0$ (articular surface) and the negative electrode at $z = \omega$, Eq. (3) is intergrated from δ to 0,

$$\hat{V}(\omega) = -\int_{\delta}^{0} \frac{k_{21}}{k\ k_{22}}\hat{U}(z,\omega)dz \tag{4}$$

where $\hat{V}(\omega)$ and $\hat{U}(z,\omega)$ are the complex amplitudes corresponding to the sinusoidal steady state. If the velocity profile $\hat{U}(z,\omega)$ can be measured or calculated, then the streaming potential $\hat{V}(\omega)$ can be computed and compared to experimental results.

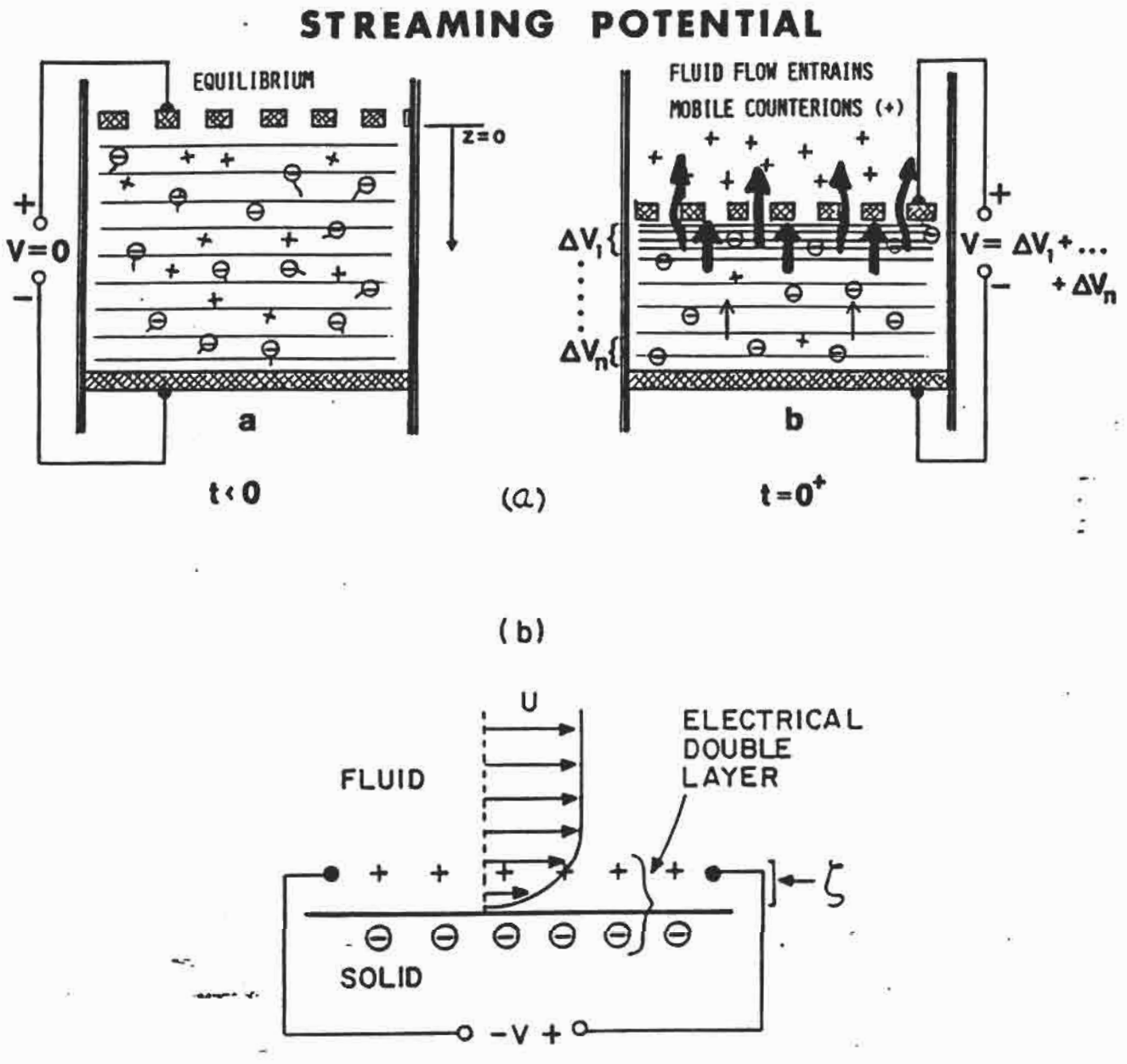
STREAMING POTENTIAL
EQUILIBRIUM
z=0
V=0
a
t<0
(a)
FLUID FLOW ENTRAINS
MOBILE COUNTERIONS (+)
ΔV1
ΔVn
V= ΔV1 + ... + ΔVn
b
t=0+
(b)
U
FLUID
ELECTRICAL DOUBLE LAYER
ζ
SOLID
-V +

Figure 1.3.1 :

To estimate the velocity profile, the fundamental equations of poroelasticity are combined as described in Section 8.2. As cartilage is deformed, the internal electrical potential and fluid velocity fields will vary with position inside the matrix in a manner that must be consistent with the internal deformation and stress fields. The velocity and deformation fields are related by continuity, Eq. (8.2.8) (assuming that the fluid and solid phases are each incompressible),

$$U(z,\omega) = -j\omega\hat{u}(z,\omega) \tag{5}$$

The displacement profile was solved for the case of sinusoidal steady state uniaxial confined compression to predict the of Eq. (5) for bulk cartilage. In addition, a lumped parameter spring constant K_s was included to account for observed properties of the porous platen and the local three-dimensional interdigitation between the cartilage surface and the porous filter connected to the load cell:

$$\hat{u}(z,\omega) = u_o \left(\frac{(K_s/A)}{(K_s/A) + H\gamma \coth \gamma\delta} \right) \frac{\sinh \gamma(\delta - z)}{\sinh \gamma\delta} \tag{6}$$

where A is the specimen cross-sectional area, H is the matrix equilibrium elastic modulus, γ is the complex wavenumber $(1+j)[\omega/2Hk]\delta$ is the specimen thickness, and u_o is the imposed dynamic displacement. For $f < 0.01$ to 0.1 Hz, it was found that $K_s/A \gg H\gamma\delta \coth \gamma\delta$ and the term in brackets in Eq. (6) becomes unity. The displacement field (6) corresponds to a diffusion wave characterized by the skin depth $(2Hk/\omega)$. The sinusoidal streaming potential amplitude and phase angle ψ corresponding to the displacement field (6) was obtained by using Eqs. (5) and (6) in Eq. (4),

$$\hat{V}(\omega) = \frac{-j\omega u_o k_{21}}{\gamma k k_{22}} \frac{K_s/A}{K_s/A + H\gamma \coth \gamma\delta} \frac{\cosh \gamma\delta - 1}{\sinh \gamma\delta} \tag{7}$$

$$\psi = \gamma \angle \hat{V}(\omega) \tag{8}$$

The theoretical model for streaming potential, Eqs. (7) and (8) has been compared to deformation induced potentials measured across plugs of bovine articular cartilage in uniaxial confined compression. Specimens from the femoropatellar groove were tested from 0.001 Hz to 20 Hz. The mechanical stiffness, mechanical phase angle between stress and displacement, and the electrical potential and its phase angle were compared to the corresponding mechanical theory. By curve fitting the mechanical theory to data, H, k and K_s were computed for each specimen (Figure 8.3.2a). This

is important since the electrical phase angle ψ (Eq. (8)) contains no other adjustable parameters. The reasonable fit between experimental and theoretical ψ over the entire frequency range (Figure 8.3.2b) was interpreted as very strong evidence that the deformation-induced potentials were produced by a streaming (electrokinetic) mechanism. Hence, use of the simultaneous measurement of streaming potential can provide important information on velocity and deformation fields within articular cartilage, subjected to various mechanical deformations.

A powerful technique for isolating transduction mechanism is to characterize its kinetics. Here, the kinetics of the measured potentials are embodied in the electrical phase angle ψ, which was compared to a macrocontinuum theoretical model based on the flow of fluid relative to a charged matrix. A significant piezoelectric response in cartilage would be highly unlikely due to macroscopic symmetry considerations, and due to the fast charge relaxation time constants (10^{-7} to 10^{-9} sec).

It could be hypothesized that pulse-like mechanical deformations in wet bone and cartilage may produce an initial piezoelectric spike followed by a more slowly varying streaming potential response. However, successful detection of even nanosecond potential spikes is not conclusive evidence of a piezoelectric mechanism because the frequency response of a streaming mechanism in a microporous medium may also be very high. An order of magnitude estimate of the latter can be computed from the viscous diffusion time constant $\tau_{\text{v.d.}}$ associated with the onset of full-developed creeping flow in a capillary of radius R. Given fluid viscosity η and density ρ, dimensional analysis of the Navier-Stokes equation gives

$$\tau_{\text{v.d.}} \simeq \frac{\rho^2}{\eta} \tag{9}$$

where $\tau_{\text{v.d.}} \sim 10^{-6} - 10^{-10}$sec for $R = 10^{-6} - 10^{-8}$m respectively. Since the streaming potential mechanism is usually based on the assumption of viscous dominated creeping flow, may be taken as a measure of the frequency response of this mechanism.

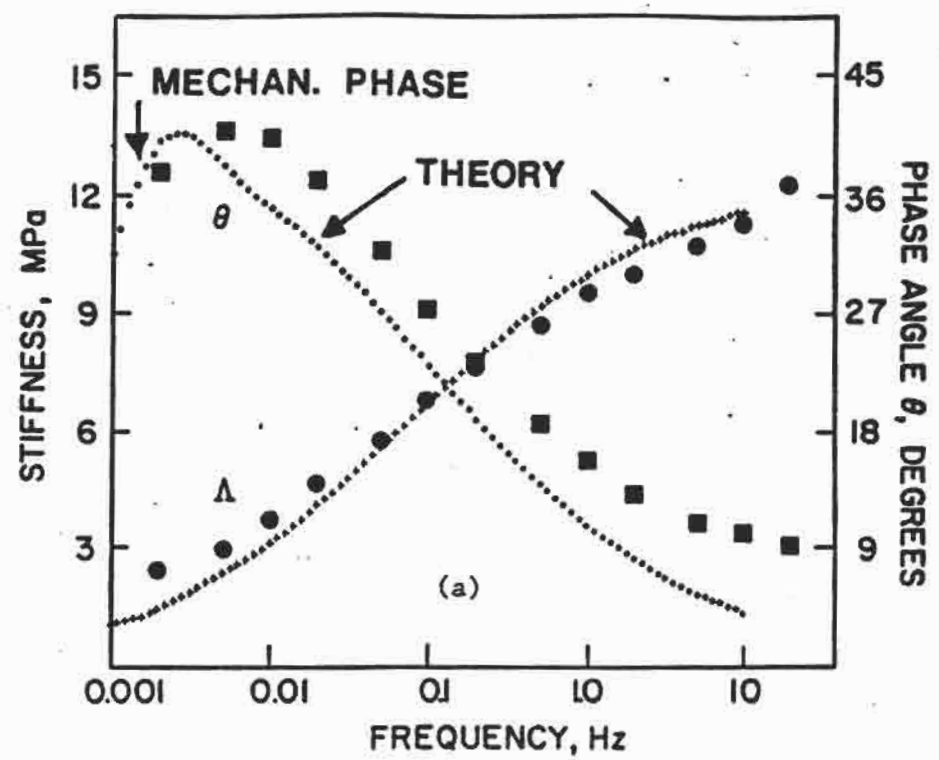
MECHAN. PHASE
THEORY
θ
Λ
(a)
STIFFNESS, MPa
PHASE ANGLE θ, DEGREES
15
12
9
6
3
45
36
27
18
9
0.001
0.01
0.1
1.0
10
FREQUENCY, Hz

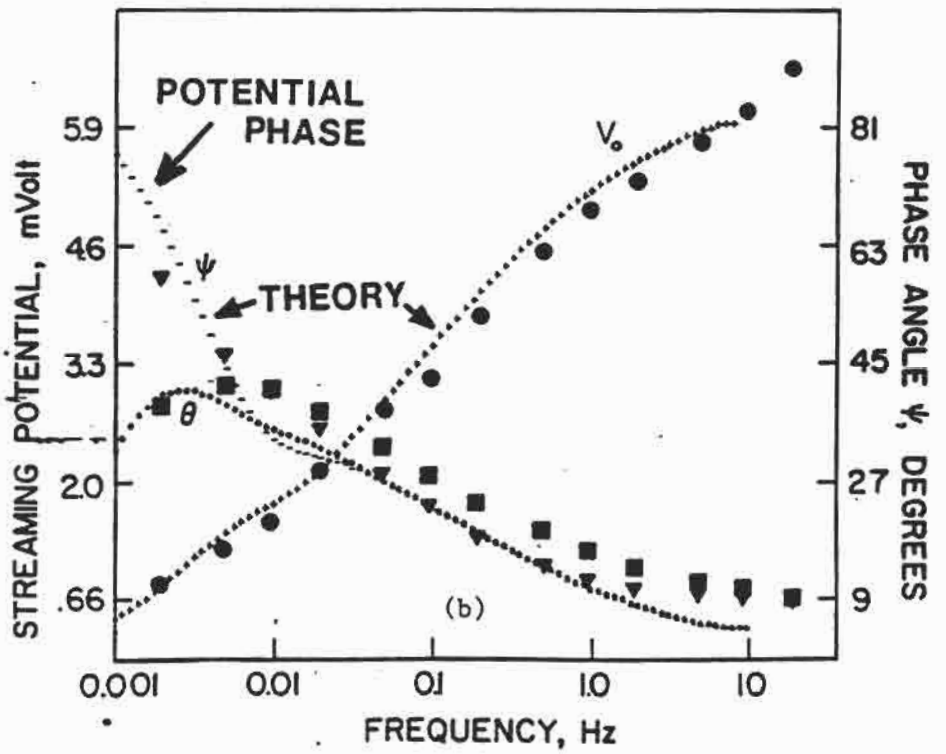
POTENTIAL
PHASE
THEORY
Ψ
θ
V_o
(b)
STREAMING POTENTIAL, mVolt
PHASE ANGLE Ψ, DEGREES
59
46
33
20
.66
81
63
45
27
9
0.001
0.01
0.1
1.0
10
FREQUENCY, Hz

Figure 8.3.2 :